

Two Manganese Halide Hybrids Based on 1-Butyl-2,3-dimethylimidazolium: Synthesis, Crystal Structure and Photoluminescence^①

CHENG Min^{a, b} JIN Jian-Ce^b
LI Jian-Rong^b ZHANG Zhi-Zhuan^{a, b}
GONG Liao-Kuo^{b②} HUANG Xiao-Ying^{b②}

^a (College of Chemistry and Materials Science, Fujian Normal University, Fuzhou 350007, China)

^b (State Key Laboratory of Structural Chemistry, Fujian Institute of Research on the Structure of Matter, Chinese Academy of Sciences, Fuzhou 350002, China)

ABSTRACT Two new inorganic-organic hybrid manganese(II) halide crystals, namely [BMMIm]₂[MnCl₄] (**1**, BMMIm = 1-butyl-2,3-dimethylimidazolium) and [BMMIm]₂[MnBr₄] (**2**), have been obtained simply by heating/stirring with nearly 100% yield. Single-crystal X-ray diffraction (SCXRD) study reveals that **1** crystallizes in triclinic space group of $P\bar{1}$ with $a = 10.0176(7)$, $b = 14.9603(11)$, $c = 12.9086(8)$ Å, $\alpha = 91.060(4)^\circ$, $\beta = 110.204(5)^\circ$, $\gamma = 92.361(4)^\circ$, $V = 1235.19(12)$ Å³, $Z = 2$, $D_c = 1.353$ g cm⁻³, $F(000) = 526$, $\mu = 0.978$ mm⁻¹, $R = 0.0410$ and $wR = 0.0690$ ($I > 2\sigma(I)$) and $M_r = 503.23$; **2** belongs to orthorhombic space group of $P2_12_12_1$ with $a = 10.0176(7)$, $b = 14.9603(11)$, $c = 17.4450(14)$ Å, $V = 2614.4(3)$ Å³, $Z = 4$, $D_c = 1.730$ g cm⁻³, $F(000) = 1340$, $\mu = 6.629$ mm⁻¹, $R = 0.0440$ and $wR = 0.0520$ ($I > 2\sigma(I)$) and $M_r = 681.07$. The ionic compounds **1** and **2** are composed of mononuclear tetrahedral [MnX₄]²⁻ anion and two ionic liquid cations of [BMMIm]⁺. The photoluminescence (PL) of **1** and **2** was characterized and the influence of halogen atom types on PL was investigated.

Keywords: manganese halide, ionic liquid, organic-inorganic hybrid, crystal structure, luminescence property;

DOI: 10.14102/j.cnki.0254-5861.2011-3089

1 INTRODUCTION

Manganese(II)-based inorganic-organic hybrid metal halides show excellent properties such as ferroelectricity^[1, 2] and luminescence^[3, 4]. The manganese(II) ion can form [MnX_n]²⁻ⁿ anions (X = halogen) which then crystallize with various organic cations to generate manganese(II) halide based ionic compounds. The 3d⁵ electron configuration of Mn²⁺ endows such ionic compounds with the emission originating from the ⁴T₁ → ⁶A₁ radiative transition, which can be easily influenced by the coordination environment of Mn²⁺^[3, 4]. Generally, green and red/pink emission is observed for the compounds with tetrahedrally^[5, 6] and octahedrally coordinated^[1, 2, 7] manganese(II) ions, respectively. It is worth noting that the organic cations in such ionic compounds are mostly protonated organic amines^[3, 4]. Ionic liquids (ILs)

have a wide operating temperature range as well as good thermal stability and chemical stability^[8, 9]. In addition, ILs are usually colorless and possess little absorption in visible and near-infrared regions, which makes them ideal as the host for luminescent materials^[10, 11]. Furthermore, ionic liquid cations (ILCs) could induce many weak interactions. The interactions between the ILCs and [MnX₄]²⁻ (X = Cl or Br) anions, such as ionic interactions^[12], hydrogen bonds^[6] and anion ···π interactions^[13], have vital influences on the assembly of various supramolecular structures. For example, [A]₂[MnBr₄] (A = N-butyl-N-methylpyrrolidinium and N-butyl-N-methylpiperidinium) possess the photoluminescent quantum yields (PLQY) of 80.9% and 54.5%, respectively; different ILCs could regulate the hydrogen bonding between anions and cations, thus regulating the PLQY^[6]. In this article, we used the imidazole-based ionic

Received 6 January 2021; accepted 21 February 2021 (CCDC 2053551 for **1** and 2053550 for **2**)

① Supported by the National Natural Science Foundation of China (No. 21671187) and the Natural Science Foundation of Fujian Province (No. 2020J01118)

② Corresponding authors. E-mails: lkong@fjirsm.ac.cn and xyhuang@fjirsm.ac.cn

liquid [BMMIm]X (BMMIm=1-butyl-2,3-dimethylimidazolium, X = Cl, Br) to synthesize two new inorganic-organic hybrid crystals with green emission, namely [BMMIm]MnX₄ (X = Cl for **1**, Br for **2**). The PLQY for **1** is 53.65%, while that for **2** is 81.36%. In these compounds, the H-bond, anion $\cdots\pi$ and C-H $\cdots\pi$ interactions are present among [BMMIm]⁺ cations and [MnX₄]²⁻ anions, leading to a three-dimensional supramolecular framework. The weak interactions have been studied in detail. By adjusting the type of halogen atoms that coordinate with the Mn²⁺ ion, the PLQY of the title compounds is tuned. In syntheses, a mixture of [BMMIm]X and MnX₂ salt was simply heated under stirring to obtain the title compounds with a yield near unity. The facile and rapid synthesis is expected to be applied to the large-scale synthesis of inorganic-organic hybrid metal halide materials.

2 EXPERIMENTAL

All chemical reagents used in this study were of AR grade, which are commercially available and can be used without further purification. 1-Butyl-2,3-dimethylimidazolium chloride ([BMMIm]Cl, 99%) and 1-butyl-2,3-dimethylimidazolium bromide ([BMMIm]Br, 99%) were purchased from Lanzhou Institute of Chemical Physics, CAS (Gansu, China); manganese(II) bromide tetrahydrate (MnBr₂·4H₂O) (98.0%) was available from Acros Chem Co., LTD (Shanghai, China); manganese(II) chloride tetrahydrate (MnCl₂·4H₂O) (99.0%) was commercial from Adamas Chem Co., LTD (Shanghai, China).

Single-crystal X-ray diffraction (SCXRD) data were collected on a SuperNova CCD diffractometer with graphite-monochromated Mo-K α radiation (λ = 0.71073 Å) at 100 K. Elemental analyses (EA) were performed on a German Elementary Vario EL III instrument. Powder X-ray diffraction (PXRD) was measured on a Rigaku Miniflex-II diffractometer with Cu-K α radiation (λ = 1.54178 Å) in the 2 θ range of 5~55°. Thermogravimetric analysis (TGA) was performed on a NETZSCH STA 449F3 thermogravimetric analyzer under a N₂ atmosphere from 25 to 1200 °C at a heating rate of 10 °C·min⁻¹. Fourier-transform infrared (FTIR) spectroscopy was carried out on a Vertex 70 FTIR spectrophotometer using KBr pellets within the range of 4000~400 cm⁻¹. Photoluminescence (PL) was recorded on an Edinburgh FL980 UV/V/NIR fluorescence spectrometer. Quantum yields (QYs) for **1** and **2** were measured by Edinburgh FLS 1000 UV/V/NIR fluorescence spectrometer.

2.1 Synthesis of compound 1

Compounds **1** and **2** were synthesized by similar procedures, as shown in Fig. 1. MnCl₂·4H₂O (5 mmol) was dissolved into [BMMIm]Cl (10 mmol) at 80 °C (completely dissolved in about 2 minutes), which was naturally cooled down to room temperature under constant stirring. Light-green microcrystals of [BMMIm]₂[MnCl₄] were obtained with nearly 100% yield (**1**, Yield: 2.856 g, 99.3% based on manganese chloride, melting point: 52.4 °C). The loss of the sample during transfer process was negligible. Light-green block-like crystals suitable for SCXRD were obtained by recrystallization of **1** in ethanol. EA: calcd. for **1**: C, 42.42; N, 10.99; H, 6.46%. Found for **1**: C, 42.92; N, 11.12; H, 6.76%.

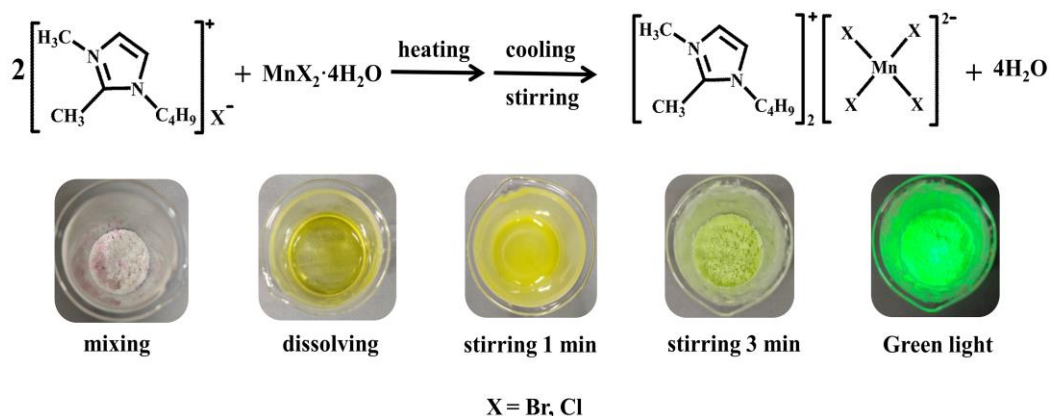


Fig. 1. Synthetic pathways of compounds **1** and **2** (up) and photo images showing the synthetic process of compound **2** (down)

2.2 Synthesis of compound 2

[BMMIm]₂[MnBr₄] was synthesized by a similar reaction for **1** except replacing [BMMIm]Cl with [BMMIm]Br and

MnCl₂·4H₂O with MnBr₂·4H₂O, respectively. Yellow-green microcrystals were obtained with a yield of 98.9% based on MnBr₂·4H₂O. Its melting point is 65.7 °C. The diagram of

synthetic process of compound **2** is depicted in Fig. 1. After recrystallization in ethanol, massive olive-green block-like crystals were produced which can be used for SCXRD. EA: calcd. for **2**: C, 31.30; N, 8.18; H, 4.93%. Found for **2**: C, 31.74; N, 8.23; H, 4.99%.

2.3 Structure refinements

The crystals of **1** (0.38mm × 0.22mm × 0.20mm) and **2** (0.53mm × 0.20mm × 0.16mm) were collected for data collection. A total of 17796 reflections were collected in the $1.99 \leq \theta \leq 30.21^\circ$ range with $R_{\text{int}} = 0.0447$, 6431 of which are independent for **1**. For **2**, 10771 total reflections were collected in $2.34 \leq \theta \leq 30.26^\circ$ with $R_{\text{int}} = 0.0380$, of which

6460 are independent. *SHELX* 2016 package was used to solve and refine the structures on F^2 by the full-matrix least-squares methods^[14]. Note that the butyl chain on one of the unique [BMMIm] of **2** is disordered over two positions with S.O.F. of 0.759(12) and 0.241(12), respectively; thus, the restraints of DFIX and SADI were applied to obtain chemically reasonable models and atomic displacement parameters. Selected bond lengths and angles, and selected hydrogen bonding data for compounds **1** and **2** are listed in Tables 1 and 2, respectively; C–H $\cdots\pi$ and anion $\cdots\pi$ interactions are shown in Table 3.

Table 1. Selected Bond Lengths (Å) and Bond Angles (°) for Compounds **1** and **2**

1		2	
Bond/Angle	Dist./°	Bond/Angle	Dist./°
Mn(1)–Cl(4)	2.3406(7)	Mn(1)–Br(2)	2.4932(11)
Mn(1)–Cl(3)	2.3509(6)	Mn(1)–Br(3)	2.5038(11)
Mn(1)–Cl(2)	2.3704(6)	Mn(1)–Br(4)	2.5076(11)
Mn(1)–Cl(1)	2.3895(6)	Mn(1)–Br(1)	2.5086(11)
Cl(4)–Mn(1)–Cl(3)	111.74(3)	Br(2)–Mn(1)–Br(3)	108.45(4)
Cl(4)–Mn(1)–Cl(2)	111.52(3)	Br(2)–Mn(1)–Br(4)	114.36(4)
Cl(3)–Mn(1)–Cl(2)	109.96(2)	Br(3)–Mn(1)–Br(4)	107.21(4)
Cl(4)–Mn(1)–Cl(1)	107.28(2)	Br(2)–Mn(1)–Br(1)	109.03(4)
Cl(3)–Mn(1)–Cl(1)	109.77(2)	Br(3)–Mn(1)–Br(1)	114.33(4)
Cl(2)–Mn(1)–Cl(1)	106.39(2)	Br(4)–Mn(1)–Br(1)	103.57(4)

Table 2. Selected Hydrogen Bond Lengths (Å) and Bond Angles (°) for Compounds **1** and **2**

1				
D–H \cdots A	d(D–H)	d(H \cdots A)	d(D \cdots A)	<(DHA)
C(1)–H(1A) \cdots Cl(3)#1	0.95	2.83	3.574(2)	136
C(2)–H(2A) \cdots Cl(1)#2	0.95	2.91	3.586(2)	130
C(4)–H(4A) \cdots Cl(3)#1	0.98	2.93	3.795(3)	148
C(4)–H(4C) \cdots Cl(3)#3	0.98	2.91	3.662(3)	134
C(5)–H(5B) \cdots Cl(2)#3	0.98	2.90	3.802(2)	154
C(5)–H(5C) \cdots Cl(2)	0.98	2.75	3.683(2)	159
C(6)–H(6A) \cdots Cl(4)	0.99	2.71	3.684(2)	170
C(6)–H(6B) \cdots Cl(1)#2	0.99	2.92	3.827(2)	152
C(10)–H(10A) \cdots Cl(1)#2	0.95	2.79	3.656(2)	153
C(11)–H(11A) \cdots Cl(2)#4	0.95	2.88	3.797(2)	163
C(13)–H(13C) \cdots Cl(1)	0.98	2.98	3.957(2)	175
C(14)–H(14A) \cdots Cl(1)#5	0.98	2.91	3.725(2)	141
C(14)–H(14C) \cdots Cl(3)#5	0.98	2.83	3.717(2)	151
2				
D–H \cdots A	d(D–H)	d(H \cdots A)	d(D \cdots A)	<(DHA)
C(1)–H(1A) \cdots Br(4)#1	0.93	3.02	3.785(7)	141
C(2)–H(2A) \cdots Br(2)#2	0.93	3.02	3.786(7)	141
C(4)–H(4A) \cdots Br(4)#1	0.96	2.78	3.709(7)	162
C(4)–H(4C) \cdots Br(1)	0.96	2.77	3.730(6)	174
C(5)–H(5A) \cdots Br(2)#3	0.96	2.92	3.832(6)	160
C(5)–H(5B) \cdots Br(1)	0.96	2.93	3.877(6)	170
C(5)–H(5C) \cdots Br(3)#4	0.96	2.95	3.748(7)	142

To be continued

C(6)–H(6A)··Br(3)#2	0.97	3.04	3.949(7)	157
C(10)–H(10A)··Br(4)#3	0.93	2.94	3.758(7)	147
C(13)–H(13A)··Br(4)#3	0.96	3.00	3.871(7)	151
C(13)–H(13B)··Br(1)	0.96	3.06	4.009(6)	171
C(14)–H(14A)··Br(1)	0.96	3.06	3.850(6)	140

Symmetry transformations used to generate the equivalent atoms:

#1: $x, y-1, z$; #2: $-x+1, -y+1, -z+1$; #3: $-x+1, -y+1, -z$; #4: $x-1, y, z$; #5: $-x+1, -y+2, -z+1$

Table 3. C–H··· π and Anion··· π Interactions for Compounds 1 and 2

1					
Y–X (I)··Cg (J)	ARU (J)	X··Cg (Å)	Y–X··Cg (°)	Y··Cg (Å)	Y–X, Pi
C–H··· π interactions					
C(13)–H(13B)→Cg(1)	2666	2.74	137	3.5202(2)	47
C(18)–H(18A)→Cg(1)	2565	2.95	128	3.6301(2)	52
Anion··· π interactions					
Mn(1)–Cl(4)→Cg(2)	2666	3.6326	132	5.4866(3)	23
2					
Y–X (I)··Cg (J)	ARU (J)	X··Cg (Å)	Y–X··Cg (°)	Y··Cg (Å)	Y–X, Pi
C–H··· π interactions					
C(4)–H(4B)→Cg(1)	4755	2.88	117	3.4273(3)	31
Anion··· π interactions					
Mn(1)–Br(2)→Cg(1)	1555	3.7074	123	5.4693(4)	16

[2666] = $1-x, 1-y, 1-z$; [2565] = $-x, 1-y, -z$; [4755] = $2-x, 1/2+y, 1/2-z$

3 RESULTS AND DISCUSSION

3.1 Discussion on crystal structures

SCXRD reveals that compound **1** belongs to space group $P\bar{1}$ while **2** is of space group $P2_12_12_1$. The asymmetric units for both compounds consist of two [BMMIm]⁺ cations and one [MnX₄]^{2−} (X = Cl for **1**, Br for **2**) anion, as shown in Fig. 2. The unique Mn²⁺ in both compounds is four-coordinated with X[−] (X = Cl, Br) ion, forming a distorted tetrahedral configuration. The butyl chains in the two [BMMIm]⁺ cations for both compounds, however, adopt different conformations. Selected torsion angles (°) for compound **1**: N(2)–C(6)–C(7)–C(8), 68.8(3); C(6)–

C(7)–C(8)–C(9), 67.5(3); N(4)–C(15)–C(16)–C(17), 60.7(3) and C(15)–C(16)–C(17)–C(18), 175.7(2); for compound **2**: N(2)–C(6)–C(7)–C(8), −57.1(8); C(6)–C(7)–C(8)–C(9), −58.6(8); N(4)–C(15)–C(16)–C(17), −71.0(10); C(15)–C(16)–C(17)–C(18), −176.0(10); N(4)–C(15)–C(16B)–C(17B), 168(3) and C(15)–C(16B)–C(17B)–C(18B), −147(3). Apparently, they are GG and GT modes, respectively^[15]. Note that the disordered part of N(4)–C(15)–C(16B)–C(17B)–C(18B) adopts a TG mode. The distances of Mn–X bonds are in the range of 2.3406(7)~2.3895(6) Å for **1** and 2.4932(11)~2.5086(11) Å for **2**, in agreement with the Mn–X bond lengths of the previously reported manganese halide hybrids^[3, 4, 6, 16].

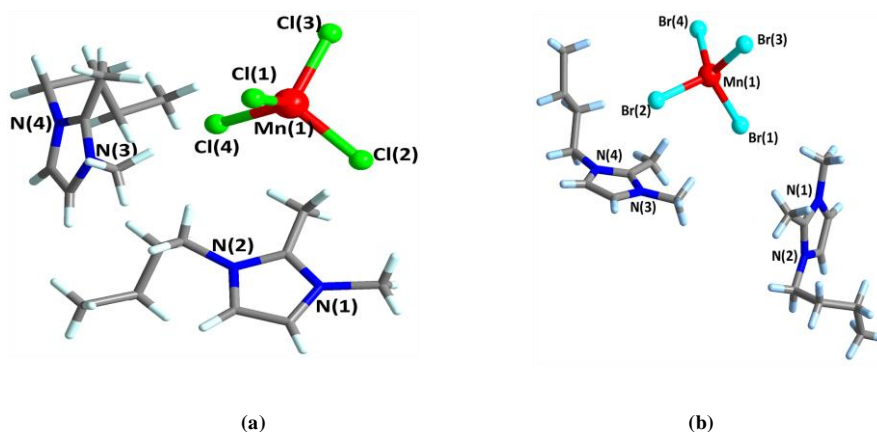


Fig. 2. Asymmetric units of compounds **1** (a) and **2** (b). One of the disordered butyl chain in the N(3)/N(4) moiety of **2** is omitted for clarity

In compound **1**, hydrogen bond interactions result in a three-dimensional supramolecular framework (Fig. 3a). The hydrogen bonding environment for each $[\text{MnCl}_4]^{2-}$ is shown in Fig. 3b. Additionally, the adjacent $[\text{BMMIm}]^+$ cations are connected to form a one-dimensional chain through $\text{C-H} \cdots \pi$ interaction, and interact with the $[\text{MnCl}_4]^{2-}$ anions through anion $\cdots \pi$ interactions (Fig. 3c).

Similarly, in **2** the hydrogen bonds also lead to a three-dimensional supramolecular framework (Fig. 4a). The hydrogen bonding environment for each $[\text{MnBr}_4]^{2-}$ is shown in Fig. 4b. However, the $[\text{MnBr}_4]^{2-}$ anion and two $[\text{BMMIm}]^+$ cations are connected to each other by $\text{C-H} \cdots \pi$ and anion $\cdots \pi$ interaction to form an isolated $[\text{BMMIm}]_2[\text{MnBr}_4]$ unit (Fig. 4c).

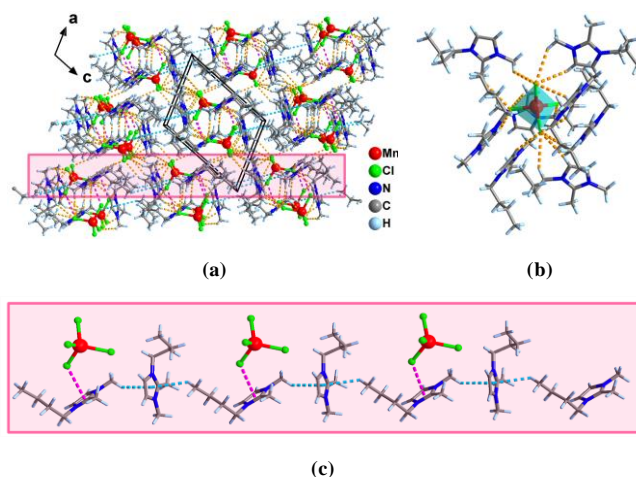


Fig. 3. (a) View of the packing diagram of **1** with H-bond, anion $\cdots \pi$, and $\text{C-H} \cdots \pi$ interactions. The H-bond interaction is highlighted in yellow dotted-line, the anion $\cdots \pi$ interaction in magenta dotted-line, and the $\text{C-H} \cdots \pi$ interaction in blue dotted-line. (b) The hydrogen bonding environment around the $[\text{MnCl}_4]^{2-}$ anion. (c) $\text{C-H} \cdots \pi$ interactions and anion $\cdots \pi$ interaction of **1** between the cations and anions

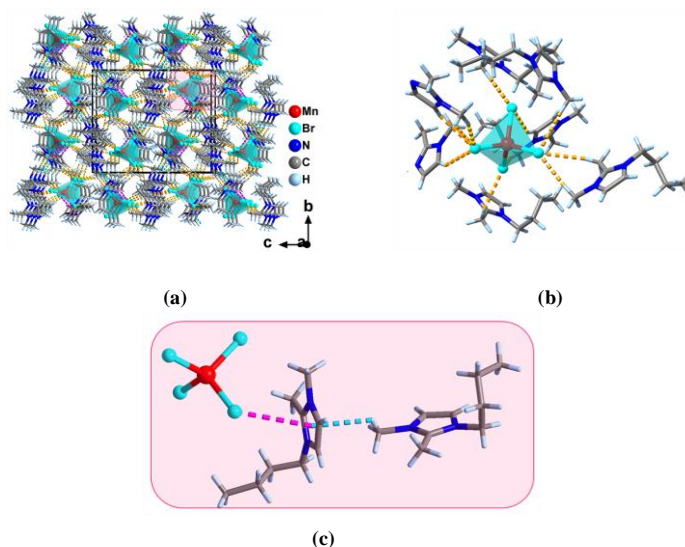


Fig. 4. (a) View of the packing diagram of **2** with H-bond (yellow dotted-line), anion $\cdots \pi$ (magenta dotted-line) and $\text{C-H} \cdots \pi$ interactions (blue dotted-line). (b) The hydrogen bonding environment around the $[\text{MnBr}_4]^{2-}$ anion. (c) $\text{C-H} \cdots \pi$ interactions and anion $\cdots \pi$ interaction of **2** between cations and anions

The different H-bond patterns between $[\text{MnX}_4]^{2-}$ anions and the surrounding cations in the two title compounds are illustrated in Figs. 3b, 4b and Table 2 for **1** and **2**. In these two compounds, each $[\text{MnX}_4]^{2-}$ anion interacts with seven surrounding $[\text{BMMIm}]^+$ cations by hydrogen bonding, and

the $\text{H} \cdots \text{X}$ ($\text{X} = \text{Cl}$ for **1**, Br for **2**) distances fall in the ranges of $2.71 \sim 2.98$ and $2.77 \sim 3.06$ Å, respectively. In addition, as for anion $\cdots \pi$ interactions, the distances between the X atoms and the center of the electron-deficient imidazole rings are 3.71 Å for **1** and 3.63 Å for **2**.

The C–H··· π interactions in the two compounds are different, that is, two types of C–H··· π interactions could be observed for **1** while merely one for **2**.

So far, imidazole based ILs have been explored for the formation of transition metal-containing ILs, but most of them are based on di-substituted imidazolium, such as [BMIm]₂[MX₄] (M = Cu, Co, Mn, Sn, Ni, Fe, Zn, Pd and Pt)^[17–20]. However, tri-substituted imidazole ionic liquids have been rarely applied^[21]. The whole synthesis process of the title compounds took about 5 minutes, and the scale of reaction could be increased easily. In addition, there was no molecular solvent involved in the reaction. By contrast, compounds with similar structures^[17–20] needed

to be prepared by stirring for a long time (more than 1 hour), and the synthesis process required the participation of molecular solvents.

3.2 PXRD patterns, TGA and IR

The phase purity of compounds **1** and **2** was characterized by PXRD (Fig. 5). The PXRD patterns of compounds **1** and **2** are consistent with the corresponding one simulated from the SCXRD data. There is a slight deviation in the angle since the experimental PXRD patterns were recorded at room temperature while the simulated ones are based on SCXRD at 100 K. In addition, the difference in intensity of diffraction peak may be attributed to the preferred orientation of crystal growth.

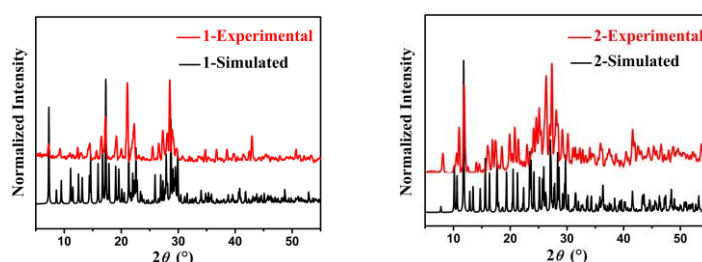


Fig. 5. PXRD patterns for **1** and **2** compared to the ones simulated from single-crystal X-ray data.

In order to investigate the thermal stability of compounds **1** and **2**, thermogravimetric tests were performed at a temperature range of 25 to 1200 °C. Compound **1** shows 74.52% (calcd.: 75.00%) of mass loss in the range of 300 ~ 550 °C (Fig. 6a), which might be due to the decomposition

of ILs. At 670 ~ 850 °C, the mass loss is 20.38%, indicating the decomposition of MnCl₂. Compound **2** lost 68.93% (calcd.: 68.55%) of its mass at 300 ~ 450 °C. The decomposition of MnBr₂ at 620 ~ 780 °C results in a mass loss of 26.74%.

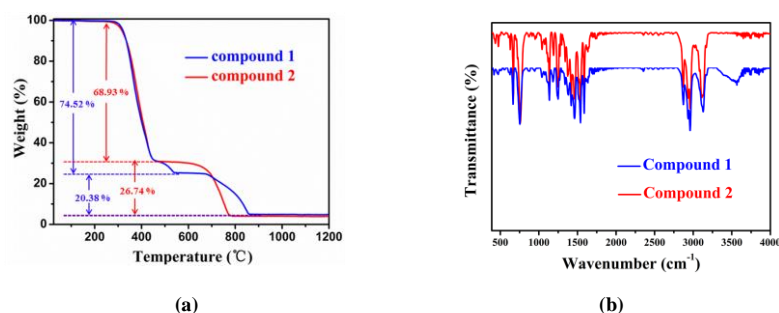


Fig. 6. TGA curves (a) and FTIR spectra (b) for compounds **1** and **2**

FTIR spectroscopy of compounds **1** and **2** (Fig. 6b) clearly demonstrates the existence of [BMMIm]⁺ cations. The two absorption peaks near 2925 and 2868 cm^{−1} should be derived from the absorption of –CH₃ and –CH₂ groups in [BMMIm]⁺^[22]. The peaks of 1498, 1300 and 1248 cm^{−1} are C=C and C=N and C–N stretching vibrations of [BMMIm]⁺ and C–H in-plane bending vibration, respectively^[23]. External bending vibration absorption positions

for C–H and C–N in [BMMIm]⁺ are 829, 734 and 658 cm^{−1}^[23, 24].

3.3 Photophysical properties

In this work, the luminescent properties of the title compounds have been measured at room temperature. As shown in Fig. 7, the emission spectra of **1** and **2** both display green emission under the irradiation of 450 nm. The green emission could be ascribed to the *d-d* ⁴T₁ → ⁶A₁ transition of

Mn(II) ion in tetrahedral $[\text{MnX}_4]^{2-}$ ($\text{X} = \text{Cl}, \text{Br}$)^[3, 4]. The energy splitting of $^4\text{T}_1$ excited state brings about three maxima bands around 275, 360, and 450 nm in the PL excitation spectra of **1** and **2** (Figs. 7a, 7c and 7e). The PL lifetime of **1** and **2** is 126.46 and 316.93 ms (Figs. 7b and 7d),

respectively, which confirms their room-temperature phosphorescence performance. Due to the heavy atom effect^[3], the two compounds have different PLQY, that is, 53.65% for **1** and 81.36% for **2**, respectively (Fig. 7f).

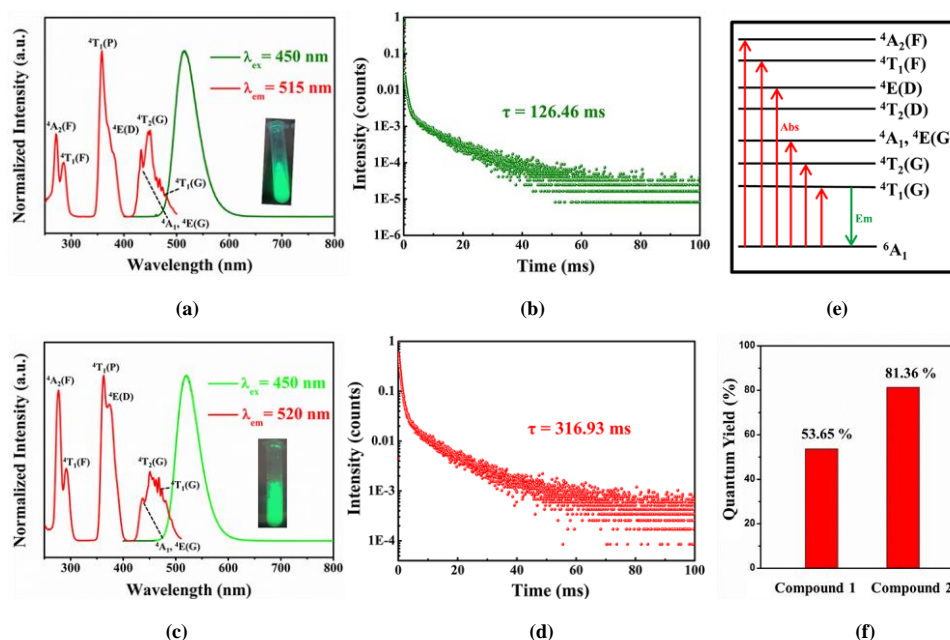


Fig. 7. Solid state excitation (red lines) and emission spectra (green lines) for compounds **1** (a) and **2** (c). The time-resolved photoluminescence decays of solid-state compounds **1** (b) and **2** (d) at room temperature. (e) Schematic diagram showing the energy adsorption, migration, and emission process of Mn(II) complex in a tetrahedral environment. (f) The PLQYs of compounds **1** and **2**

4 CONCLUSION

In conclusion, we have synthesized two new hybrid manganese(II) halide compounds by a facile method with nearly 100% yield, and studied their structures and fluorescence properties. Optical analysis shows that both crystals

exhibit excellent luminescence properties, *e.g.*, high PLQY and long life time. Due to the heavy atom effect, the two compounds show different PLQYs. The synthesis method is simple and rapid, which is expected to be used in the large-scale synthesis of a large number of hybrid metal halide materials.

REFERENCES

- (1) Zhang, Y.; Liao, W. Q.; Fu, D. W.; Ye, H. Y.; Chen, Z. N.; Xiong, R. G. Highly efficient red-light emission in an organic-inorganic hybrid ferroelectric: (pyrrolidinium) MnCl_3 . *J. Am. Chem. Soc.* **2015**, 137, 4928–4931.
- (2) Ye, H. Y.; Zhou, Q.; Niu, X.; Liao, W. Q.; Fu, D. W.; Zhang, Y.; You, Y. M.; Wang, J.; Chen, Z. N.; Xiong, R. G. High-temperature ferroelectricity and photoluminescence in a hybrid organic-inorganic compound: (3-pyrrolinium) MnCl_3 . *J. Am. Chem. Soc.* **2015**, 137, 13148–13154.
- (3) Tao, P.; Liu, S. J.; Wong, W. Y. Phosphorescent manganese(II) complexes and their emerging applications. *Adv. Opt. Mater.* **2020**, 2000985–21.
- (4) Qin, Y.; She, P.; Huang, X.; Huang, W.; Zhao, Q. Luminescent manganese(II) complexes: synthesis, properties and optoelectronic applications. *Coord. Chem. Rev.* **2020**, 416, 213331–19.
- (5) Morad, V.; Chernikh, I.; Pottschacher, L.; Shynkarenko, Y.; Yakunin, S.; Kovalenko, M. V. Manganese(II) in tetrahedral halide environment: factors governing bright green luminescence. *Chem. Mater.* **2019**, 31, 10161–10169.
- (6) Gong, L. K.; Hu, Q. Q.; Huang, F. Q.; Zhang, Z. Z.; Shen, N. N.; Hu, B.; Song, Y.; Wang, Z. P.; Du, K. Z.; Huang, X. Y. Efficient modulation of photoluminescence by hydrogen bonding interactions between inorganic $[\text{MnBr}_4]^{2-}$ anions and organic cations. *Chem. Commun.* **2019**, 55, 7303–7306.
- (7) Wu, Y. X.; Wang, C. F.; Li, H. H.; Jiang, F.; Shi, C.; Ye, H. Y.; Zhang, Y. Highly efficient and uncommon photoluminescence behavior combined with multiple dielectric response in manganese(II) based hybrid phase transition compounds. *Eur. J. Inorg. Chem.* **2020**, 2020, 394–399.

- (8) Rogers, R. D.; Seddon, K. R. Ionic liquids-solvents of the future? *Science* **2003**, 302, 792–793.
- (9) Wilkes, J. S. A short history of ionic liquids - from molten salts to neoteric solvents. *Green Chem.* **2002**, 4, 73–80.
- (10) Li, H.; Liu, P.; Shao, H.; Wang, Y.; Zheng, Y.; Sun, Z.; Chen, Y. Green synthesis of luminescent soft materials derived from task-specific ionic liquid for solubilizing lanthanide oxides and organic ligand. *J. Mater. Chem.* **2009**, 19, 5533–5540.
- (11) Li, H.; Shao, H.; Wang, Y.; Qin, D.; Liu, B.; Zhang, W.; Yan, W. Soft material with intense photoluminescence obtained by dissolving Eu_2O_3 and organic ligand into a task-specific ionic liquid. *Chem. Commun.* **2008**, 5209–5211.
- (12) Shen, N. N.; Cai, M. L.; Song, Y.; Wang, Z. P.; Huang, F. Q.; Li, J. R.; Huang, X. Y. Supramolecular organization of $[\text{TeCl}_6]^{2-}$ with ionic liquid cations: studies on the electrical conductivity and luminescent properties. *Inorg. Chem.* **2018**, 57, 5282–5291.
- (13) Garcia-Saiz, A.; de Pedro, I.; Migowski, P.; Vallcorba, O.; Junquera, J.; Blanco, J. A.; Fabelo, O.; Sheptyakov, D.; Waerenborgh, J. C.; Fernandez-Diaz, M. T.; Rius, J.; Dupont, J.; Gonzalez, J. A.; Fernandez, J. R. Anion- π and halide-halide nonbonding interactions in a new ionic liquid based on imidazolium cation with three-dimensional magnetic ordering in the solid state. *Inorg. Chem.* **2014**, 53, 8384–8396.
- (14) Sheldrick, G. M. Crystal structure refinement with *SHELXL*. *Acta Crystallogr. Sect. C* **2015**, 71, 3–8.
- (15) Laus, G.; Bentivoglio, G.; Kahlenberg, V.; Wurst, K.; Nauer, G.; Schottenberger, H.; Tanaka, M.; Siehl, H. U. Conformational flexibility and cation-anion interactions in 1-butyl-2,3-dimethylimidazolium salts. *Cryst. Growth Des.* **2012**, 12, 1838–1846.
- (16) Mao, L.; Guo, P.; Wang, S.; Cheetham, A. K.; Seshadri, R. Design principles for enhancing photoluminescence quantum yield in hybrid manganese bromides. *J. Am. Chem. Soc.* **2020**, 142, 13582–13589.
- (17) Zehbe, K.; Kollosche, M.; Lardong, S.; Kelling, A.; Schilde, U.; Taubert, A. Ionogels based on poly(methyl methacrylate) and metal-containing ionic liquids: correlation between structure and mechanical and electrical properties. *Int. J. Mol. Sci.* **2016**, 17, 391–16.
- (18) Kozlova, S. A.; Verevkin, S. P.; Heintz, A.; Peppel, T.; Koeckerling, M. Paramagnetic ionic liquid 1-butyl-3-methylimidazolium tetrabromidocobaltate(II): activity coefficients at infinite dilution of organic solutes and crystal structure. *J. Chem. Eng. Data* **2009**, 54, 1524–1528.
- (19) Zhong, C.; Sasaki, T.; Jimbo-Kobayashi, A.; Fujiwara, E.; Kobayashi, A.; Tada, M.; Iwasawa, Y. Syntheses, structures, and properties of a series of metal ion-containing dialkylimidazolium ionic liquids. *Bull. Chem. Soc. Jpn.* **2007**, 80, 2365–2374.
- (20) Zhong, C. M.; Zuo, Y. J.; Jin, H. S.; Wang, T. C.; Liu, S. Q. Bis(1-n-butyl-3-methylimidazolium) tetrabromopalladate(II). *Acta Crystallogr. Sect. E* **2006**, 62, M2281–M2283.
- (21) Kolle, P.; Dronskowski, R. Hydrogen bonding in the crystal structures of the ionic liquid compounds butyldimethylimidazolium hydrogen sulfate, chloride, and chloroferrate(II, III). *Inorg. Chem.* **2004**, 43, 2803–2809.
- (22) Du, C. F.; Li, J. R.; Huang, X. Y. Microwave-assisted ionothermal synthesis of SnSe_x nanodots: a facile precursor approach towards SnSe_2 nanodots/graphene nanocomposites. *RSC Adv.* **2016**, 6, 9835–9842.
- (23) Chowdhury, A.; Thynell, S. T. Confined rapid thermolysis/FTIR/ToF studies of imidazolium-based ionic liquids. *Thermochim. Acta* **2006**, 443, 159–172.
- (24) Polat, T.; Yildirim, G. Investigation of solvent polarity effect on molecular structure and vibrational spectrum of xanthine with the aid of quantum chemical computations. *Spectrochim. Acta A* **2014**, 123, 98–109.